Nano Research
2023, 16(3): 3913–3923

ISSN 1998-0124 CN 11-5974/O4
https://doi.org/10.1007/s12274-022-4866-5

Review Article

Bioinspired directional liquid transport induced by the corner effect

Zhongyu Shi[1], Zhongxue Tang[1], Bojie Xu[1], Lei Jiang[1,2], and Huan Liu[1,2] (✉)

[1] *Key Laboratory of Bio-Inspired Smart Interfacial Science and Technology of Ministry of Education, School of Chemistry, Beihang University, Beijing 100191, China*
[2] *Research Institute for Frontier Science, Beihang University, Beijing 100191, China*

Received: 29 May 2022 / **Revised:** 8 July 2022 / **Accepted:** 3 August 2022

ABSTRACT

Many natural creatures have demonstrated unique abilities in directional liquid transport (DLT) for better adapting to the local environment, which, for a long time, have inspired the material fabrication for applications in microfluidics, self-cleaning, water collection, etc. Recently, DLTs aroused by the corner effect have been witnessed in various natural organisms, where liquid transports/spreads spontaneously along the corner structures in microgrooves, wedges or conical structures driven by micro-/nano- scaled capillary forces without external energy input. Particularly, these DLTs show advantages of ultrahigh speed, continuous proceeding, and/or external controllability. Here, we reviewed recent research advances on the bioinspired DLTs induced by the corner effect, as well as the involved mechanisms and the artificial counterpart materials with various applications. We also introduced some bioinspired materials that are capable of stimulus-responsive DLT under external fields. Finally, we suggested perspectives of the bioinspired DLTs in liquid manipulations.

KEYWORDS

directional liquid transport, bioinspired materials, corner effect, capillary rise, Laplace pressure

1 Introduction

Many natural organisms have developed the unique capability of directional liquid transport (DLT) during long-term evolution [1–5]. As has been well documented, surface micro-/nano-structures, distributed in either an anisotropic or an asymmetric pattern, play crucial roles for the DLT due to the ability in breaking the symmetry of the tri-phase contact line (TCL) [6–8]. The as-generated Laplace pressure difference drives liquid transport without any external energy input. For example, both the cactus spine [1] and the spider silk [2] enable efficient water/fog collection, by taking advantage of the DLTs on their conical spines and spindle-knots, respectively. So far, the conical structure has served as the most frequent used media for the DLT, as has been witnessed in various biological and/or artificial materials [9–12]. To be noticed, the corner structures, especially those with gradient open angles, have shown outstanding ability in driving DLTs [13–17], which regretfully has been little reviewed in the last decade.

As shown in Fig. 1, many natural organisms capable of DLTs are benefited from their unique corner structures. The duck-billed microcavities on the peristome surface of *Nepenthes alata* enable a continuous and long-distance DLT, by which a slippery surface was maintained [13]. Imparted by the ratchets with dual-reentrant topography, liquids with different surface tensions on the *Araucaria* leaf transport to different directions [6]. Various corner structures capable of DLTs have been reported, such as goose feathers with anisotropic wedges in each microchannel [14], dual cylindrical hairs with wet-rebuilt open-wedges [15], the *Sarracenia* trichomes with multi-scale microchannels on conical fibers [16], and bamboo fibers with hierarchical micro-/nano- channels [17]. In general, DLTs induced by the corner effect refer to the spontaneous liquid transport with a preferred direction in wedges, microgrooves, or corners under either capillary forces or Laplace pressures. Efforts on deep understanding the DLTs [18–23] would inspire innovative applications in water collection [24–29], oil/water separation [30–32], lubrication [33, 34], self-cleaning [35, 36], medical detection [37–40], heat transfer [41–44], and microfluidics [45–49].

Here, we reviewed recent research progresses on bioinspired DLTs induced by the corner effect, including the representative natural organisms, the involved mechanisms, the biomimetic materials, and those with external-stimulus responsive DLTs. We also suggested the perspectives in liquid manipulations.

2 Driving forces of the DLT induced by the corner effect

Natural organisms have evolved various DLT systems with diverse corner structures, such as wedges, cones, and channels, which enable the Laplace pressure difference by the asymmetric liquid curvatures confined by structures. The as-generated capillary forces at micro-/nano- scale promote the liquid transport directionally until reaching an equilibrium, showing the importance of the corner effect in DLT [50–54]. The structure confinement is a benefit for breaking the symmetry of the TCL,

Address correspondence to liuh@buaa.edu.cn

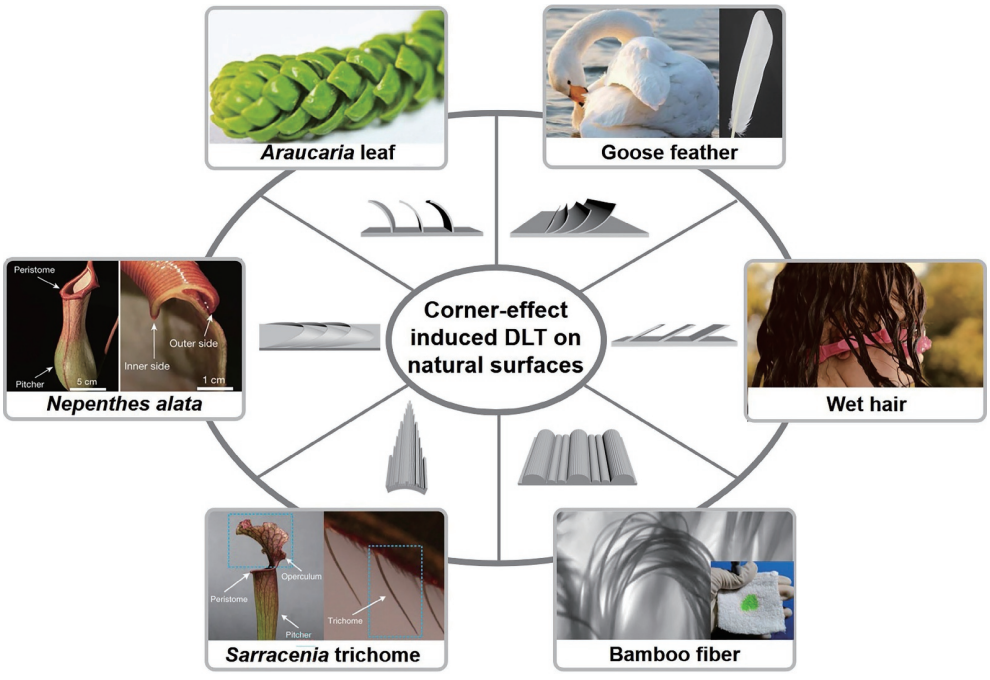

Figure 1 Corner effect induced DLTs in various natural organisms and the correspondent model structures: *N. alata*, *Araucaria* leaf, goose feathers, wet hairs, bamboo fibers, and *Sarracenia* trichomes. Reproduced with permission from Ref. [13], © Macmillan Publishers Limited 2016; Ref. [6], © Feng, S. L. et al., some rights reserved; exclusive licensee American Association for the Advancement of Science. No claim to original U.S. Government Works 2021; Ref. [14], © Wiley-VCH GmbH 2021; Ref. [17], © Wiley-VCH GmbH 2021; Ref. [16], © Springer Nature 2018 and the Internet.

which therefore triggers the DLT.

The corner structure with proper topology facilitates both the forward spreading and the backward pinning for the DLT. As shown in Fig. 2(a), the forward spreading of liquid normally proceeds along an open inner corner, which can be ascribed to the capillary rise in the wedge angle. The capillary rising height $H(x)$ at the intersecting corner of two vertical placed plates can be calculated by the balance between the gravitational potential and interfacial potential, expressed as [13]

$$H(x) = \frac{2\gamma\cos\theta}{\rho g x \alpha_1} + \frac{\alpha_1 - \alpha_2}{\alpha_1 h} H^2(x) \quad (1)$$

where γ, ρ, θ, α, g, h, and $H(x)$ indicate the liquid surface tension, liquid density, contact angle, opening angle, the gravitational acceleration, the height of the intersecting plates, and the height of the liquid surface at position x, respectively. The $H(x)$ gradually increases when reducing the θ or supplying $\alpha_1 > \alpha_2$. It indicates that the gradient wedge corner is more conducive for the liquid spreading.

On the other hand, the conical structure with an asymmetric axial radius causes Laplace pressure difference, which drives liquid transport from the high curvature side (tip) towards the low curvature side (base) spontaneously (Fig. 2(b)) [55–58]. The Laplace force can be expressed as [1]

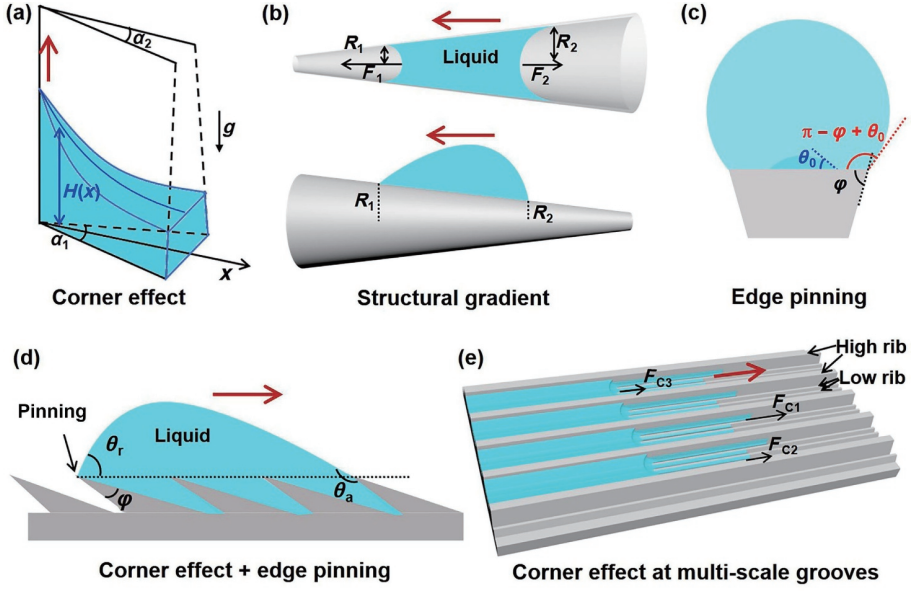

Figure 2 Schematic illustration of the driving forces for liquid transport. (a) Capillary rise along wedge corner. (b) Liquid transport along conical structures. (c) Pinning effects when liquid meets a sharp edge. (d) DLT on the anisotropic structured surface with periodic wedges under the cooperative effect of both corner effect and edge pinning. (e) Liquid spreading in multiscale grooves driving by capillary forces along each corner.

$$F_{\text{Laplace}} = -\int_{R_2}^{R_1} \frac{2\gamma}{(R+R_0)^2}\sin\alpha dz \quad (2)$$

where γ represents the liquid surface tension, R is the local radius of the cone, R_1 and R_2 are the local radii of the cone at two opposite sides of a droplet, R_0 is the drop radius, α is the half apex angle of the cone, and dz is the minute incremental radius along the cone. It is worth noting that such Laplace pressure difference induced by the conical structure is also applicable for the wetting liquid in a conical tube, where a liquid is liable to transport to a higher curvature region (tip side).

Additionally, sharp edge structures can cause both wettable and nonwettable liquids pinning (Fig. 2(c)) [59]. Notably, the edge pinning effect is crucial for the DLTs, behaving as preventing backward liquid flow [60]. In detail, liquid remains pinned when its apparent contact angle θ is below $\pi - \varphi + \theta_0$, expressed as Eq. (3) [61, 62]. Here, θ_0 and φ are the inherent contact angle and the angle at the sharp edge

$$\theta \leq \pi - \varphi + \theta_0 \quad (3)$$

With the rapid progress of basic theories, new-conceptual DLT surfaces based on the corner effect have been developed. One representative example is the anisotropic structured surface with periodically arranged wedges (Fig. 2(d)). On such surface, directional and continuous liquid flow is driven by the capillary force at each wedge; while in the backward direction, the reverse flow was largely prohibited by the edge-pinning effect. Thus, under the synergetic effect of both corner effect and edge-pinning effect, DLTs proceed with no energy input. Moreover, the corner effect has been observed frequently on the surface with micro-/nano-channels. As shown in Fig. 2(e), ribs with different heights and widths are distributed at intervals on the surface with open micro-/nano-channels, which makes the multi-scale capillary forces facilitating liquid spreading [16, 63, 64]. Additionally, for liquid transport on a surface with hierarchical channels, DLT proceeds rather fast since the pre-wetted surface can largely decrease the resistance.

3 Natural DLTs driven by the corner effect

As an important mass/energy transfer approach, DLTs driven by either the enhanced capillary rise or multi-scale capillary forces along various corner structures have been recently observed on many biological organisms for better habitat to local environments, such as peristome surface of *N. alata*, goose feathers, *Araucaria* leaves, wet-rebuilt dual-hairs, *Sarracenia* trichomes, and bamboo fibers.

3.1 DLTs driven by the capillary rise along wedge corners

3.1.1 *The peristome surface of N. alata*

The tropical plant *N. alata* has evolved a lubricated pitcher for efficient catching insects [65]. Chen et al. [13] revealed the continuous liquid transport on the peristome surface of *N. alata* (NPS, Fig. 3(a)), which was characterized by two-order hierarchical parallel grooves with each microgroove textured as arch-shaped microcavities. Such unique structures make numerous gradient wedged corners, which helps to generate a gradient capillary force for continuous driving upward liquid

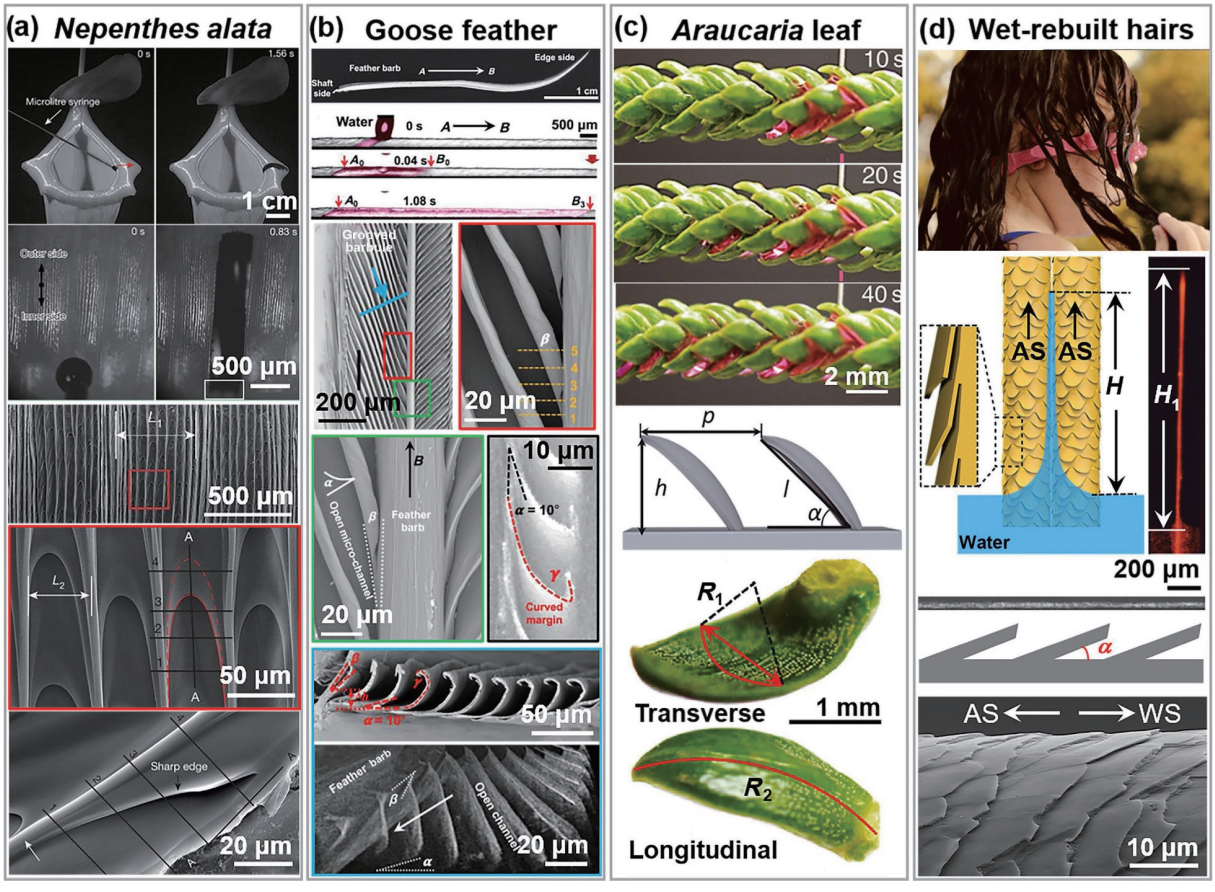

Figure 3 Natural DLTs based on the corner effect of unique micro-/nano- structures. (a) DLT on the peristome surface of *N. alata*. Reproduced with permission from Ref. [13], © Macmillan Publishers Limited 2016. (b) DLT on goose feather. Reproduced with permission from Ref. [14], © Wiley-VCH GmbH 2021. (c) DLT on *Araucaria* leaf. Reproduced with permission from Ref. [6], © The American Association for the Advancement of Science 2021. (d) DLT on wet-rebuilt dual-hairs. Reproduced with permission from Ref. [15], © Wiley-VCH GmbH 2021.

transfer [66, 67]. While in the opposite direction, the liquid is liable to be pinned at sharp edges of the microcavities. Therefore, DLT proceeds continuously with no observable backward flow, which offers inspiration for the fabrication of stable lubricated surfaces.

3.1.2 *Goose feathers*

Bird feathers possess numerous corner structures consisting of barbules and barbs [68–70]. Luan et al. [14] revealed a self-cleaning behavior on the goose feather based on the transient superhydrophilicity endowed by the saliva coating on its unique anisotropic corner structures (Fig. 3(b)). The grooved barbule aligns on the barb with a gradient wedge angle β. Each grooved barbule is curved laminas and overlaps with adjacent laminas, forming a semi-open concave microchannel with a wedge angle α. Capillary rises along both types of wedge corners facilitate the long-distance DLT on the goose feather, which enables thorough self-cleaning contaminates trapping within the textures.

3.1.3 *Araucaria leaves*

Directional steering of liquid on *Araucaria* leaf has been revealed very recently [6], which is attributable to the unique three-dimensional (3D) capillary ratchets (Fig. 3(c)). The *Araucaria* leaf consists of periodically arranged asymmetric ratchets with a title angle α, where each ratchet takes a transverse curvature R_1 and a longitudinal curvature R_2. Such aligned and inclined array of asymmetric ratchets enables low-surface-tension liquid (ethanol) spread along the ratchet-tilting direction and high-surface-tension liquid (water) spread to the opposite direction. Such structural curvature helps to achieve long-distance DLT and well-controlled directional steering.

3.1.4 *Wet-rebuilt dual cylindrical hairs*

For the DLTs on cylindrical fibers [71–73], liquid transport along the longitude axis with no preferred direction was driven by the capillary force. Meng et al. [15] revealed that dual cylindrical hairs are capable of DLT in the against-scale (AS) direction but pinned at the edges of scales (Fig. 3(d)), which can be ascribed to the wet-rebuilt open-wedged squamae. It is proposed that open-wedges are helpful for generating the capillary force along wedge corners, with sharp edges of scales pinning the liquid in the with-scale direction. The result suggests a novel model fibrous structure for the DLTs.

3.2 DLTs driven by capillary forces along corners in micro-/nano-channels

3.2.1 *Sarracenia trichome*

The tropical plant *Sarracenia* has an outstanding liquid transport capacity. Chen et al. [16] found the ultrafast DLT on the trichomes of *Sarracenia* that is composed of conical fibers covered with hierarchical microchannels along the longitudinal direction (Fig. 4(a)). Its trichome is conically shaped with a length of 1,530 μm. Each trichome is covered with capillary channels at multiple scales, fabricated by two different ribs of high ribs and low ribs. In detail, from the tip to the base of the trichome, the number of low ribs between two adjacent high ribs gradually increased from 0 to 1–2 and 4–5. The Laplace pressure difference induced by the conical trichome drives the DLT of condensed fog toward its root. Meanwhile, the capillary force along the micro-/nano-channels helps form a water film to reduce the surface resistance, consequently accelerating the DLT speed. Notably, the DLT speed on a wet trichome is 11,738 μm/s, which is about 3 orders of magnitude faster than that on the cactus spine.

3.2.2 *Bamboo fibers*

Fabrics made of bamboo fibers are well-known for their self-cleaning performance, where the oil dirty can be easily washed off by water without using any surfactants. The self-cleaning is attributable to the long-term super-amphiphilicity of bamboo fibers [17]. As shown in Fig. 4(b), numerous ridges and grooves

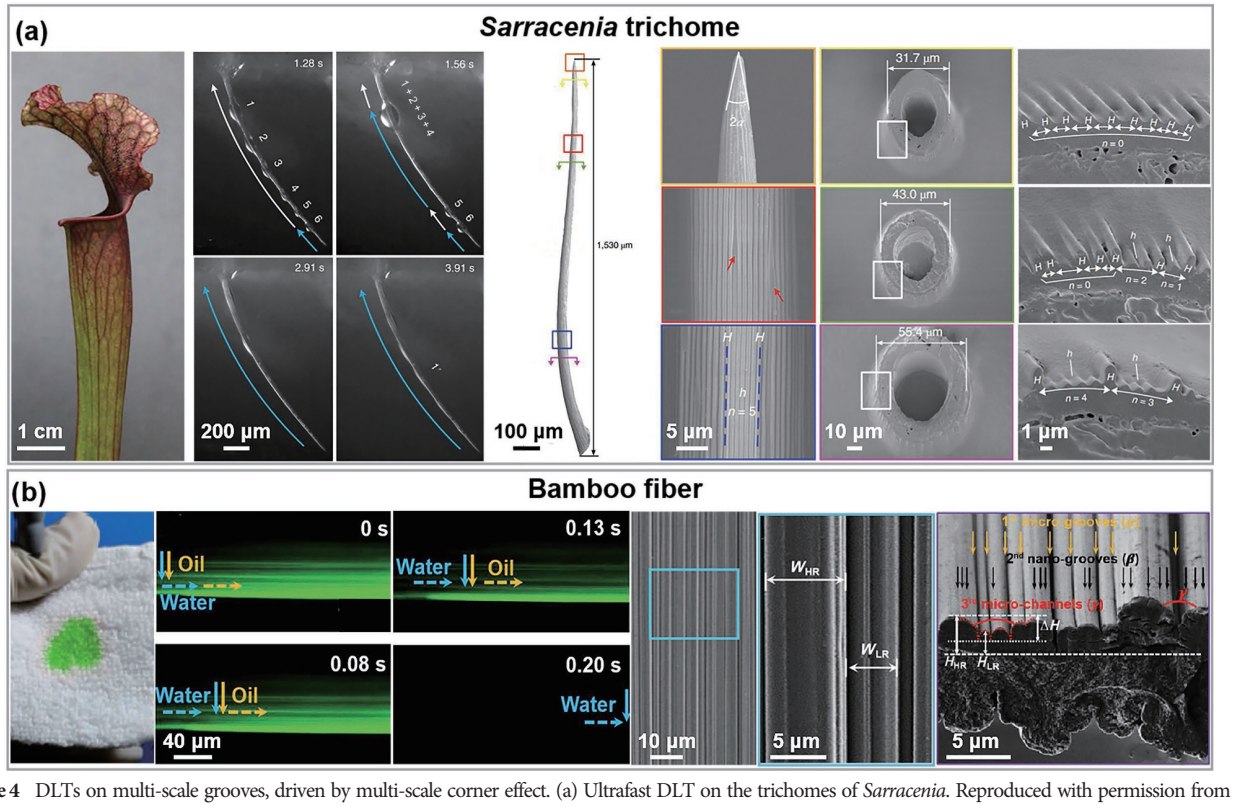

Figure 4 DLTs on multi-scale grooves, driven by multi-scale corner effect. (a) Ultrafast DLT on the trichomes of *Sarracenia*. Reproduced with permission from Ref. [16], © Springer Nature 2018. (b) Super-spreading on bamboo fibers. Reproduced with permission from Ref. [17], © Wiley-VCH GmbH 2021.

were distributed along the longitude direction of the fiber. Such hierarchical micro-/nano-grooved structure facilitates generating multi-scale capillary forces. Based on the minimization of the free energy, the pre-wetted oil can be spontaneously removed away by water flow, resulting in spontaneous self-cleaning.

4 Bioinspired materials for DLTs

Drawing inspiration from these natural surfaces that are capable of DLTs, many artificial counterpart materials with different corner structures have been developed from both organic and inorganic compounds (Table 1).

Inspired by the long-term stable lubricating surface of the NPS, several flexible polyvinyl alcohol (PVA) substrates with arrayed microcavities slant on the surface have been prepared by combining the 3D printing and replicating techniques [74]. When the PVA substrates were C-shape or S-shape bended, DLTs proceed along the C- or S- shaped trace, respectively (Fig. 5(a)). The speed of DLT was controlled by altering both the bending direction and bending radius. Such biomimetic substrates are applicable further for making a raindrop-shielding device.

Inspired by the wet-rebuilt dual-hairs, dual parallel cylindrical fibers with side-by-side arrangement were fabricated, where each single fiber was textured into oriented open-wedges [15]. The dual parallel fibers enable a controllable DLT. Upon changing the wedged angle α, the DLT behavior can be finely tuned, as a consequence of varying both the capillary force and the retention force (Fig. 5(b)). Such DLT on dual cylindrical fibers is applicable to fabricating functional textiles for managing the moisture adsorption and sweating.

Surface textures with special curvatures can be used to attract or repel liquids. The *Araucaria* leaf-inspired surface with several arrays of parallel ratchets has been prepared using 3D printing [6], on which directionally transporting water–ethanol mixtures (Fig. 5(c)) were observed. The direction of the capillary forces aroused by the 3D topology is highly dependent on the surface tension of liquids. The mixture with 40% ethanol (liquid-philic) transported forward, whereas that with 10% ethanol (poor liquid-philic) transported backward. Therefore, liquid with different surface tension flow on the surface exhibits well-controlled directional steering, self-propulsion, high velocity, and long-distance transport.

Inspired by the goose feather, a bionic feather composing of the long micro-wedge with a fixed small corner and a short micro-wedge with a 3D gradient (Fig. 5(d)) was developed, which shows a typical DLT behavior [14]. The wedged corner enables liquid transport in a preferred direction, as well as liquid pinning in the opposite direction. When the fibrous surface was modified chemically, both oil and water can spread completely in a preferred direction. Consequently, oil stains can be directionally removed away by water flow, showing a typical spontaneous directional self-cleaning behavior.

Hierarchical microchannels on the surface of the *Sarracenia* trichomes help to achieve ultrafast water transport. Wang et al. [75] developed a spine with barbs and hierarchical channels for constructing a spider-web-like fog collector and a cactus-like fog collector (Fig. 5(e)). The conical structure endows the Laplace pressure difference for driving the DLT, while the wetted channels promote the DLT process. The work indicates an intelligent unit for efficient fog harvesting.

Inspired by the self-cleaning behavior of the bamboo fabrics, Xu et al. [17] developed a series of super-amphiphilic substrates with multi-scaled oriented ridges/grooves. Capillary forces with the same direction at micro-/nano-scale are therefore enabled, which endow artificial surfaces with good spontaneous self-cleaning performance (Fig. 5(f)).

5 External stimuli-responsive DLTs

When materials with stimuli-responsive properties were used for making these cornered structures, various controllable DLTs behaviors have been demonstrated under various external field stimuli including light [76–83], magnetism [84–90], temperature [91–97], surface charge [98–101], and electricity [102–106].

Light-responsive DLT. Cornered structures made of light-responsive materials offer a method for accurate, remote, contactless, and temporary liquid manipulation [76–83]. Lv et al. [76] demonstrated the photo-induced asymmetric deformation of tubular micro-actuators for manipulating fluid slugs (Fig. 6(a)). The asymmetric structure helps generate capillary forces for propelling liquid in the conical tube. All micro-actuators are made of linear liquid crystal polymers with stable mechanical properties. Transport of a variety of liquids at controlled speeds and directions is achieved by photocontrol. They further developed photo-controllable flexible microtube of a photo-deformable polycyclooctene with azobenzene and biphenyl side chains coated

Table 1 Recent advances in bioinspired materials for DLTs and external stimuli-responsive DLTs

Artificial surface	Natural model	Corner structures	Applications	References
Bioinspired NPS	The peristome surface of *N. alata*	Microgrooves with periodic duck-billed microcavities	Raindrop-shielding device	[74]
Cylindrical fibers with oriented open-wedges	Wet-rebuilt hairs	Cylindrical fibers with oriented open-wedges	Textiles for moisture adsorption and sweating	[15]
Araucaria leaf-inspired surface	*Araucaria* leaf	Arrays of 3D parallel ratchets with dual-reentrant topography	Directional liquid sheering	[6]
Bionic feathers	Goose feathers	Micro-wedge with a fixed corner/a 3D gradient corner	Self-cleaning	[14]
Spine with barbs and hierarchical channels	Cactus spine and *Sarracenia* trichome	Micro-conical spine, microchannels, and nanochannels	Fog harvesting	[75]
Bamboo-mimetic substrate	Bamboo fiber	Microchannels, microgrooves, and nanogrooves	Self-cleaning	[17]
Light-/magnetic-responsive materials	—	Conical tube	Micro-reactors, wearable microfluidics and tubular microactuators	[76, 77, 85]
Peristome–beak mimetic surface	The peristome surface of *N. alata* and the beak of the shorebird	Micro-grooves with regular parallel arch-shaped micro-cavities and overhang structures	Microfluidic device	[92]
An annular wall with grooves and the spine with thorns and gradient microchannel arrays	Cactus spine, *Sarracenia* trichome, and the *Triarrhena saccharifiora* leaf sheath	Micro-meter scaled conical spines and microchannels	Water harvesting, moisture retention and agricultural irrigation	[120]
A high–low rib-like hierarchical texture surface	*Sarracenia* trichome	Microchannels	Droplet removal	[121]

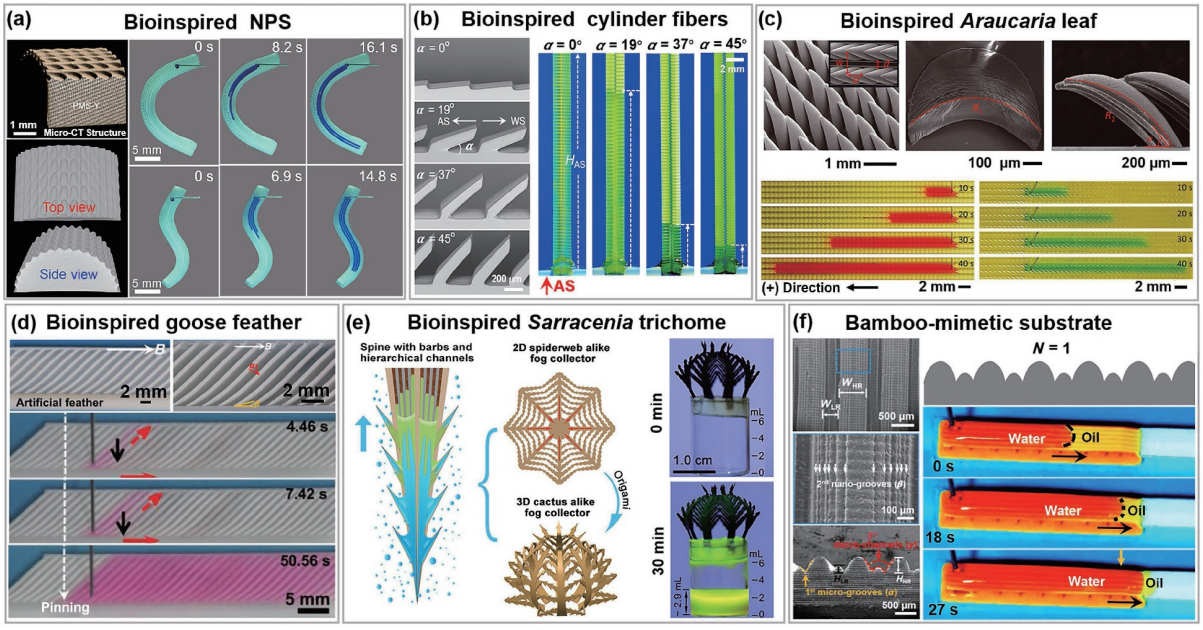

Figure 5 DLTs on various bio-inspired materials. (a) DLT on the NPS-inspired surface with a tortuous path. Reproduced with permission from Ref. [74], © American Chemical Society 2018. (b) DLT on dual cylinder fibers with wedge corner. Reproduced with permission from Ref. [15], © Wiley-VCH GmbH 2021. (c) DLTs of liquids with different surface tension on the *Araucaria* leaf-inspired surface. Reproduced with permission from Ref. [6], © The American Association for the Advancement of Science 2021. (d) DLT on the goose feather-inspired surface and its spontaneous self-cleaning behavior. Reproduced with permission from Ref. [14], © Wiley-VCH GmbH 2021. (e) The *Sarracenia* trichomes-inspired system for efficient fog collection. Reproduced with permission from Ref. [75], © American Chemical Society 2020. (f) Spontaneous self-cleaning on the bamboo fiber-inspired surface. Reproduced with permission from Ref. [17], © Wiley-VCH GmbH 2021.

in an ethylene-vinyl acetate (EVA) copolymer tube [77]. Using flexible double-layer microtubes, multiple light-driven models were established for the DLT among parallel arrays and closed-loop channels, indicating the potential application in wearable microfluidics.

Magnetic-responsive DLT. Magnetic actuation of droplets has drawn extensive attention, due to its long-range action and strong control force [84–90]. Cao et al. [84] designed an asymmetric ferromagnetic microcilia surface coating with lubricated oil. The directionality of ferromagnetic fibers can be synergistically switched by regulating the external magnet field, facilitating a continuous and omnidirectional-controllable water delivery. Lei et al. [85] developed a magnetic tubular micro-actuator (Fig. 6(b)). The micro-actuator can be asymmetrically deformed by the external magnetic field, inducing a Laplace pressure difference. Thus, droplets can move toward the narrow end in an additive-free method.

Thermal-responsive DLT. Temperature gradient, which can be prepared quantitatively by external stimulus, drives the DLT towards the low-temperature area due to the as-generated gradient in the surface tension [91–97]. Li et al. [91] reported a special DLT process on a topological surface with U-shaped islands and divergent side-channels against the temperature gradient (Fig. 6(c)). For a positive temperature gradient, droplets can directionally move towards the hot region at a slow speed, driven by the corner effect. When reversing the direction of the temperature gradient, the co-effect of a negative temperature gradient and the corner effect accelerates the DLT process.

DLT driven by the surface charge gradient. Surface charge gradient has been used as an efficient method for realizing the ultrafast and long-distance DLT on superhydrophobic surfaces [98–101]. As reported, a specific path with a surface charge density gradient can be facilely printed by impacting droplets on a superhydrophobic silica nano-coating and continuously changing the impact height [98]. The maximum movement speed of a droplet is as high as 1.1 m/s along the printed path toward the charge gradient (Fig. 6(d)). This work greatly extends the application of both DLT and superhydrophobic materials.

Electric-responsive DLT. Electric-responsive DLT is a fast-response liquid manipulation strategy by changing the surface chemistry [102–106]. Wang et al. [102] revealed an *in-situ* reversible superwetting transition on a binary Cu/Sn micro-/nano-textures between underwater superoleophilicity and superoleophobicity by a general electrochemical strategy. In such way, an oil droplet could easily be pinned when applying the potential (underwater superoleophilicity). The droplet rolls along the inclined substrate when removing the potential (underwater superoleophobicity, Fig. 6(e)). It represents a smart material for manipulating liquid in various applications.

6 Applications of DLTs

The corner structure enables a capillary force for liquid transport in a certain direction, while its sharp edge helps to pin liquid in the opposite direction. These bio-inspired DLT devices have demonstrated various good performances in liquid harvesting, microfluidic tube, liquid separation, single-cell analysis, micro-reactor, self-cleaning, fog collection, and droplet removal (Fig. 7).

6.1 Corner structure for the controllable DLTs

Liquid harvesting. Water collection and fog harvesting are important due to the worldwide water shortage [1, 13, 107]. Inspired by the NPS, a multi-curvature structure by reasonably integrating the ratchets, concavities, and arch channels was developed (Fig. 7(a)) [108]. Droplets nucleate on the ratchet teeth and transport directionally along the curved peristome. The collector with multi-scaled curvature enables the harvesting and transporting of water, ethylene glycol, kerosene, and isopropanol, which is applicable for various fields.

Microfluidic tube. Efficient liquid manipulation is of great significance in biochemical analysis and microfluidics [109–112]. Li et al. [109] developed a micro-cavity array to control water elevation by bending the bionic plate into tubes (Fig. 7(b)). Under the co-operative effect of both peristome-mimetic structures and tube curvature, a "candy cane" shaped pipe endows a self-siphon

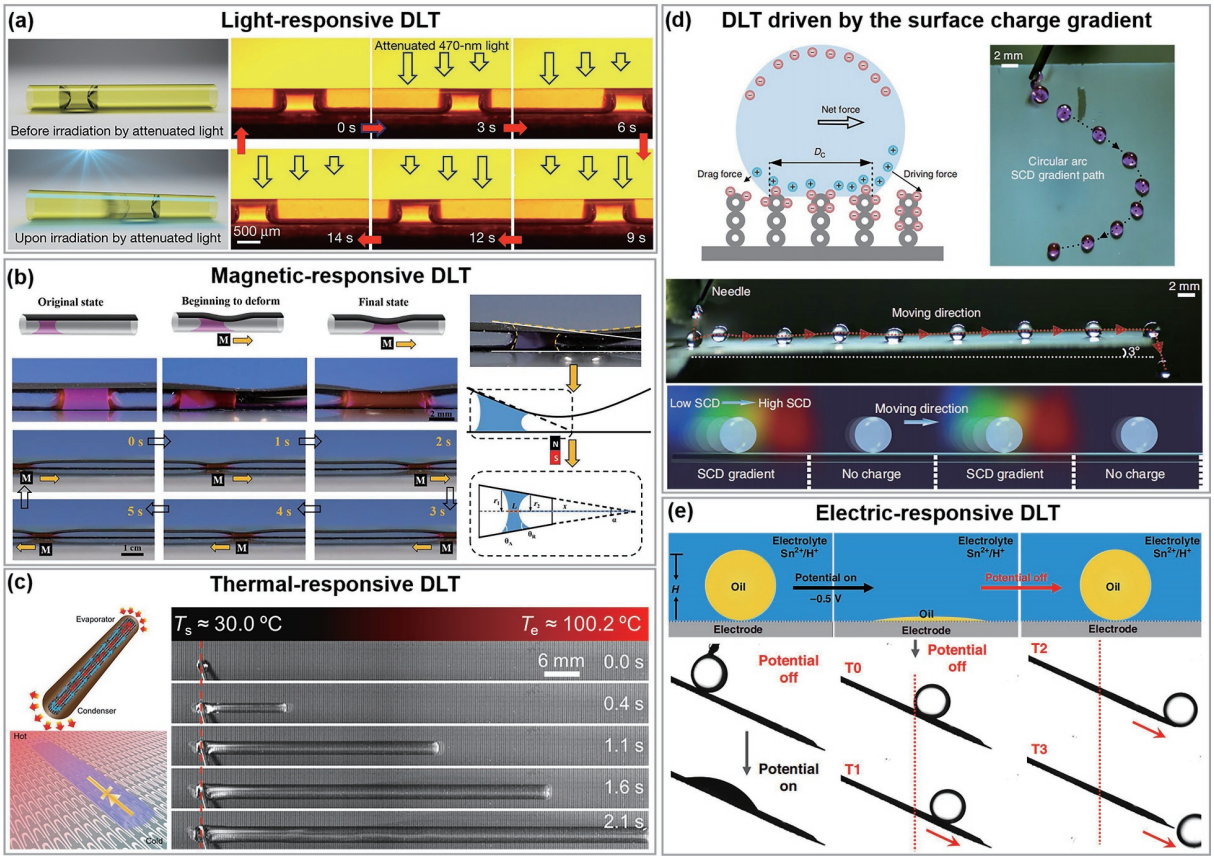

Figure 6 External-stimulus DLTs and their performance in controlling liquid transport. (a) Light-responsive DLT of the silicone oil slug. Reproduced with permission from Ref. [76], © Macmillan Publishers Limited, part of Springer Nature 2016. (b) Magnetic-responsive DLT of a liquid droplet in confined tube. Reproduced with permission from Ref. [85], © The American Association for the Advancement of Science 2018. (c) Thermal-responsive DLT of a water stream on the topological surface imposed with a negative temperature gradient. Reproduced with permission from Ref. [91], © American Chemical Society 2021. (d) DLT driven by the gradient of surface charge. Reproduced with permission from Ref. [98], © Sun, Q. Q. et al. 2019. (e) Electric-responsive liquid motion. Reproduced with permission from Ref. [102], ©Wang, Q. B. et al. 2019.

with liquid diode behavior. The water elevation height increases with decreasing the inner diameter of the tubes. It inspires next generation water transport devices.

Liquids separation. Li et al. [113] proposed a peristome-mimetic curved surface with a "saw-tooth" microcavity array for the spontaneous and directional separation of micro-meter scaled water-in-oil droplets (Fig. 7(c)). The overlapped microcavities promote liquid spreading, while the overhang structures at the rear side prevent the backward overflow. On this basis, they fabricated an arched device by integrating a convex surface of hydrophobic polydimethylsiloxane and a concave surface of hydrophilic polyvinyl alcohol. Notably, the bionic device even allows to separate oil-in-oil droplets with a surface tension difference of 14.7 mN/m, demonstrating the range of applicable liquids for micro-scaled separation.

Single-cell analysis. Rapid processing of large numbers of micro-objects is essential in molecular biology and biomedicine [114–116]. Capillary microfluidics enables the preprogrammed liquid transport relying on the geometry and surface chemistry of the microstructure [117]. Peng et al. [37] fabricated the biomimetic NPS with parallel microgrooves for ultrafast microdroplet generation and high-density microparticle arraying. By controlling the inclination angles of the substrate, microdroplets and particles can be easily arranged in these cavities (Fig. 7(d)). Meanwhile, the biomimetic NPS can be further applied to capture single cells in microdroplets.

Micro-reactor. For the lossless DLT of a droplet on periodic structures, the directional contraction of the backward spreading liquid strip is in demand [118, 119]. Zhou et al. [118] reported the controllable droplets transfer on a peristome-mimetic surface with periodic microcavities array by the asymmetrical growth and rupture of bubbles. When modifying the pressure with vacuuming, the liquid strip can levitate directionally with the assistance of bubbles. Thus, a micro-reactor is constructed by the biomimetic surface (Fig. 7(e)).

6.2 Multi-scale grooves promote the liquid spreading

Self-cleaning. Drawing inspiration from the spontaneous self-cleaning property of the bamboo fabrics, Xu et al. [17] fabricated a series of artificial substrates with multi-scale oriented micro-/nano-grooves by 3D printing (Fig. 7(f)). The micro-grooves, nano-grooves, and microchannels on the surface generate multiple capillary forces, which drive the super-spreading of water among these textures and the rapidly removing of oil contamination. The textured substrate shows good cleaning ability, suggesting a facile method for designing the long-term stable self-cleaning system.

Fog collection. Tang et al. [120] developed a bionic wearable fog collector composed of an annular wall with grooves and the spine with thorns and gradient microchannel arrays (Fig. 7(g)). The conical structures and gradient channels endow a difference in Laplace pressure, which drives a continuous DLT of the condensed fog. The fog drops were absorbed into the thin wall, which can be further used for the moisture retention of the fresh flower.

Droplet removal. A superhydrophobic trichome-mimetic substrate has been developed for the fog collection (Fig. 7(h)) [121]. Compared with the low-adhesion superhydrophobic surface, fog droplet prefers to nucleate on the superhydrophobic surface with high adhesion. Taking advantage of the high ribs

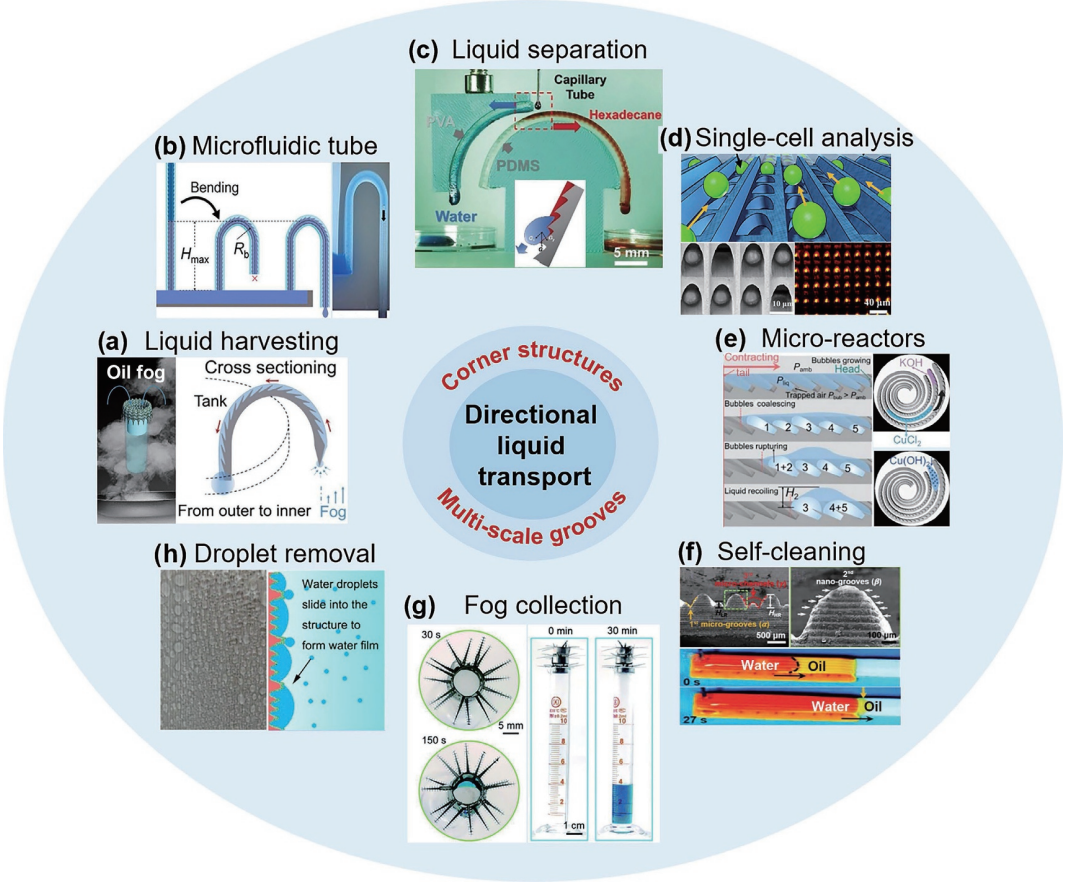

Figure 7 Representative applications of bioinspired DLT materials, including (a) liquid harvesting (reproduced with permission from Ref. [108], © Li, C. X. et al. 2020); (b) microfluidic tube (reproduced with permission from Ref. [109], © Li, C. X. et al. 2019); (c) liquid separation (reproduced with permission from Ref. [113], © Wiley-VCH GmbH & Co. KGaA, Weinheim 2017); (d) single-cell analysis (reproduced with permission from Ref. [37], © American Chemical Society 2020); (e) micro-reactors (reproduced with permission from Ref. [118], © WILEY-VCH GmbH & Co. KGaA, Weinheim 2020); (f) self-cleaning (reproduced with permission from Ref. [17], © Wiley-VCH GmbH 2021); (g) fog collection (reproduced with permission from Ref. [120], © The Royal Society of Chemistry 2021); (h) droplet removal (reproduced with permission from Ref. [121], © American Chemical Society 2020).

resisting the liquid penetration process, the condensed dew rapidly grows into a big droplet. Consequently, the gravity drives a big droplet self-removing into the collector with little residue on the superhydrophobic surface. The result expands the application of superhydrophobic surfaces in fog harvesting for alleviating the shortage of water resources.

7 Summary and outlook

As we have highlighted in this review, both natural and artificial DLT systems by the corner effect have been largely fuelled recently. To date, many DLTs have applied in water/air and oil/air systems. Wedged structures and multi-scaled grooves as two typical corner structures help generate Laplace pressure difference and capillary force at multi-scales. Consequently, numerous functional devices have been developed for various applications, such as liquid collection, liquid separation, responsive self-cleaning, single-cell analysis, micro reaction platform, and microfluidics.

External fields (such as light, magnetic, heat, and electric) help achieve smart and responsive DLT devices with little requirement of topography structures. However, there are still some challenges. For instance, developing a facile method for the fabrication of multi-scale and large-area corner structures is key to widening the practical application of DLT devices. Especially, reasonable design of corner structures can help produce DLT surfaces with good physical stability and pollution resistance, reaching the requirement of the long-term operation in complex environments. Further, we can study the DLT of other fluids (such as ionic liquid, hydrogen, or carbon dioxide) and the DLT under extreme conditions (such as extremely low or high temperature). For example, the corner structures can help form a continuous and directional liquid flow on a hot surface, consequently reaming a high heat exchange efficiency. Moreover, discovering numerous diverse DLT systems in natural creatures may enlighten new applications. The new generation of DLT devices depends on properly combining different corner structures. The combination of stimulus-responsive materials and corner structures provides a facile strategy for the controllable DLT (a desirable direction, a programmable procedure, a high speed, and a long distance), which may be used in biological devices and microfluidic and heat-transfer systems. We hope that this review could inspire readers to uncover the advances in bionic science and to generate new and intriguing ideas for incorporating the system of DLT based on the corner effect into their research.

Acknowledgements

This work was financially supported by the National Key R&D Program of China (No. 2018YFA0704801), the National Natural Science Foundation of China for Distinguished Young Scholar (No. 22125201), and the National Natural Science Foundation of China (Nos. 21872002 and 22105013).

References

[1] Ju, J.; Bai, H.; Zheng, Y. M.; Zhao, T. Y.; Fang, R. C.; Jiang, L. A multi-structural and multi-functional integrated fog collection system in cactus. *Nat. Commun.* **2012**, *3*, 1247.

[2] Zheng, Y. M.; Bai, H.; Huang, Z. B.; Tian, X. L.; Nie, F. Q.; Zhao, Y.; Zhai, J.; Jiang, L. Directional water collection on wetted spider silk. *Nature* **2010**, *463*, 640–643.

[3] Xue, Y.; Wang, T.; Shi, W. W.; Sun, L. L.; Zheng, Y. M. Water collection abilities of green bristlegrass bristle. *RSC Adv.* **2014**, *4*, 40837–40840.

[4] Zheng, Y. M.; Gao, X. F.; Jiang, L. Directional adhesion of superhydrophobic butterfly wings. *Soft Matter* **2007**, *3*, 178–182.

[5] Roth-Nebelsick, A.; Ebner, M.; Miranda, T.; Gottschalk, V.; Voigt, D.; Gorb, S.; Stegmaier, T.; Sarsour, J.; Linke, M.; Konrad, W. Leaf surface structures enable the endemic namib desert grass *Stipagrostis sabulicola* to irrigate itself with fog water. *J. Roy. Soc. Interface* **2012**, *9*, 1965–1974.

[6] Feng, S. L.; Zhu, P. G.; Zheng, H. X.; Zhan, H. Y.; Chen, C.; Li, J. Q.; Wang, L. Q.; Yao, X.; Liu, Y. H.; Wang, Z. K. Three-dimensional capillary ratchet-induced liquid directional steering. *Science* **2021**, *373*, 1344–1348.

[7] Comanns, P.; Buchberger, G.; Buchsbaum, A.; Baumgartner, R.; Kogler, A.; Bauer, S.; Baumgartner, W. Directional, passive liquid transport: The texas horned lizard as a model for a biomimetic "liquid diode". *J. Roy. Soc. Interface* **2015**, *12*, 20150415.

[8] Parker, A. R.; Lawrence, C. R. Water capture by a desert beetle. *Nature* **2001**, *414*, 33–34.

[9] Song, J. L.; Liu, Z. A.; Wang, X. Y.; Liu, H.; Lu, Y.; Deng, X.; Carmalt, C. J.; Parkin, I. P. High-efficiency bubble transportation in an aqueous environment on a serial wedge-shaped wettability pattern. *J. Mater. Chem. A* **2019**, *7*, 13567–13576.

[10] Ju, J.; Xiao, K.; Yao, X.; Bai, H.; Jiang, L. Bioinspired conical copper wire with gradient wettability for continuous and efficient fog collection. *Adv. Mater.* **2013**, *25*, 5937–5942.

[11] Wang, Q. Q.; He, Y.; Geng, X. X.; Hou, Y. P.; Zheng, Y. M. Enhanced fog harvesting through capillary-assisted rapid transport of droplet confined in the given microchannel. *ACS Appl. Mater. Interfaces* **2021**, *13*, 48292–48300.

[12] Feng, S. L.; Wang, Q. Q.; Xing, Y.; Hou, Y. P.; Zheng, Y. M. Continuous directional water transport on integrating tapered surfaces. *Adv. Mater. Interfaces* **2020**, *7*, 2000081.

[13] Chen, H. W.; Zhang, P. F.; Zhang, L. W.; Liu, H. L.; Jiang, Y.; Zhang, D. Y.; Han, Z. W.; Jiang, L. Continuous directional water transport on the peristome surface of *Nepenthes alata*. *Nature* **2016**, *532*, 85–89.

[14] Luan, K.; He, M. J.; Xu, B. J.; Wang, P. W.; Zhou, J. J.; Hu, B. B.; Jiang, L.; Liu, H. Spontaneous directional self-cleaning on the feathers of the aquatic bird *Anser cygnoides* domesticus induced by a transient superhydrophilicity. *Adv. Funct. Mater.* **2021**, *31*, 2010634.

[15] Meng, Q. A.; Xu, B. J.; Tang, Z. X.; Wei, Y.; Jiang, L.; Liu, H. Controlling directional liquid transport on dual cylindrical fibers with oriented open-wedges. *Adv. Mater. Interfaces* **2022**, *9*, 2101749.

[16] Chen, H. W.; Ran, T.; Gan, Y.; Zhou, J. J.; Zhang, Y.; Zhang, L. W.; Zhang, D. Y.; Jiang, L. Ultrafast water harvesting and transport in hierarchical microchannels. *Nat. Mater.* **2018**, *17*, 935–942.

[17] Xu, B. J.; He, M. J.; Tang, Z. X.; Jiang, L.; Liu, H. Long-term super-amphiphilic shaped-fiber with multi-scale grooved structures: Toward spontaneous self-cleaning. *Adv. Funct. Mater.* **2021**, *31*, 2102877.

[18] Wang, Z. M.; Lu, Y.; Huang, S.; Yin, S. H.; Chen, F. J. Bamboo-joint-like platforms for fast, long-distance, directional, and spontaneous transport of fluids. *Biomicrofluidics* **2020**, *14*, 034105.

[19] Tenjimbayashi, M.; Kawamura, K.; Shiratori, S. Continuous directional water transport on hydrophobic slippery ventral skin of *Lampropeltis pyromelana*. *Adv. Mater. Interfaces* **2020**, *7*, 2000984.

[20] Lee, M.; Oh, J.; Lim, H.; Lee, J. Enhanced liquid transport on a highly scalable, cost-effective, and flexible 3D topological liquid capillary diode. *Adv. Funct. Mater.* **2021**, *31*, 2011288.

[21] Li, J. Q.; Li, Y. C.; Zheng, H. X.; Liu, M. J.; Gu, H. J.; Lu, K. Y.; Zhou, X. F.; Wang, Z. K. Strengthening unidirectional liquid pumping using multi-biomimetic structures. *Extreme Mech. Lett.* **2021**, *43*, 101144.

[22] Xu, W. Z.; Xing, Y.; Liu, J.; Wu, H. P.; Cui, Y.; Li, D. W.; Guo, D. Y.; Li, C. R.; Liu, A. P.; Bai, H. Efficient water transport and solar steam generation via radially, hierarchically structured aerogels. *ACS Nano* **2019**, *13*, 7930–7938.

[23] Li, J. Q.; Zheng, H. X.; Yang, Z. B.; Wang, Z. K. Breakdown in the directional transport of droplets on the peristome of pitcher plants. *Commun. Phys.* **2018**, *1*, 35.

[24] Liu, J.; Cao, M.; Li, L.; Xu, X.; Zheng, J.; Yao, W.; Hou, X. Bioinspired interfacial design for gravity-independent fluid transport control. *Giant* **2022**, *10*, 100100.

[25] Ju, J.; Zheng, Y. M.; Jiang, L. Bioinspired one-dimensional materials for directional liquid transport. *Acc. Chem. Res.* **2014**, *47*, 2342–2352.

[26] Zhang, S. N.; Huang, J. Y.; Chen, Z.; Lai, Y. K. Bioinspired special wettability surfaces: From fundamental research to water harvesting applications. *Small* **2017**, *13*, 1602992.

[27] Xu, T.; Lin, Y. C.; Zhang, M. X.; Shi, W. W.; Zheng, Y. M. High-efficiency fog collector: Water unidirectional transport on heterogeneous rough conical wires. *ACS Nano* **2016**, *10*, 10681–10688.

[28] Liu, L. Y.; Liu, S. Y.; Schelp, M.; Chen, X. F. Rapid 3D printing of bioinspired hybrid structures for high-efficiency fog collection and water transportation. *ACS Appl. Mater. Interfaces* **2021**, *13*, 29122–29129.

[29] Cheng, Y. Q.; Wang, M. M.; Sun, J.; Liu, M. J.; Du, B. G.; Liu, Y. B.; Jin, Y. K.; Wen, R. F.; Lan, Z.; Zhou, X. F. et al. Rapid and persistent suction condensation on hydrophilic surfaces for high-efficiency water collection. *Nano Lett.* **2021**, *21*, 7411–7418.

[30] Li, K.; Ju, J.; Xue, Z. X.; Ma, J.; Feng, L.; Gao, S.; Jiang, L. Structured cone arrays for continuous and effective collection of micron-sized oil droplets from water. *Nat. Commun.* **2013**, *4*, 2276.

[31] Cui, Z. H.; Xiao, L.; Li, Y. X.; Zhang, Y. B.; Li, G. Q.; Bai, H. Y.; Tang, X. X.; Zhou, M. L.; Fang, J. H.; Guo, L. et al. A fishbone-inspired liquid splitter enables directional droplet transportation and spontaneous separation. *J. Mater. Chem. A* **2021**, *9*, 9719–9728.

[32] Li, N.; Yu, C. L.; Si, Y. F.; Song, M. R.; Dong, Z. C.; Jiang, L. Janus gradient meshes for continuous separation and collection of flowing oils under water. *ACS Appl. Mater. Interfaces* **2018**, *10*, 7504–7511.

[33] Ji, J. W.; Jiao, Y. L.; Song, Q. R.; Zhang, Y.; Liu, X. J.; Liu, K. Bioinspired geometry-gradient metal slippery surface by one-step laser ablation for continuous liquid directional self-transport. *Langmuir* **2021**, *37*, 5436–5444.

[34] Li, X.; Li, J. Q.; Dong, G. N. Bioinspired topological surface for directional oil lubrication. *ACS Appl. Mater. Interfaces* **2020**, *12*, 5113–5119.

[35] Su, B.; Tian, Y.; Jiang, L. Bioinspired interfaces with superwettability: From materials to chemistry. *J. Am. Chem. Soc.* **2016**, *138*, 1727–1748.

[36] Chen, P.; Li, X. D.; Ma, J. F.; Zhang, R.; Qin, F.; Wang, J. J.; Hu, T. S.; Zhang, Y. L.; Xu, Q. Bioinspired photodetachable dry self-cleaning surface. *Langmuir* **2019**, *35*, 6379–6386.

[37] Peng, Z. T.; Chen, Y.; Wu, T. Z. Ultrafast microdroplet generation and high-density microparticle arraying based on biomimetic *Nepenthes* peristome surfaces. *ACS Appl. Mater. Interfaces* **2020**, *12*, 47299–47308.

[38] Zarei, M. Advances in point-of-care technologies for molecular diagnostics. *Biosens. Bioelectron.* **2017**, *98*, 494–506.

[39] Charmet, J.; Arosio, P.; Knowles, T. P. J. Microfluidics for protein biophysics. *J. Mol. Biol.* **2018**, *430*, 565–580.

[40] Li, H. L.; Liu, P.; Kaur, G.; Yao, X.; Yang, M. S. Transparent and gas-permeable liquid marbles for culturing and drug sensitivity test of tumor spheroids. *Adv. Healthc. Mater.* **2017**, *6*, 1700185.

[41] Cho, H. J.; Preston, D. J.; Zhu, Y. Y.; Wang, E. N. Nanoengineered materials for liquid–vapour phase-change heat transfer. *Nat. Rev. Mater.* **2017**, *2*, 16092.

[42] Chen, X. M.; Wu, J.; Ma, R. Y.; Hua, M.; Koratkar, N.; Yao, S. H.; Wang, Z. K. Nanograssed micropyramidal architectures for continuous dropwise condensation. *Adv. Funct. Mater.* **2011**, *21*, 4617–4623.

[43] Wang, R.; Wu, F. F.; Yu, F. F.; Zhu, J.; Gao, X. F.; Jiang, L. Anti-

vapor-penetration and condensate microdrop self-transport of superhydrophobic oblique nanowire surface under high subcooling. *Nano Res.* **2021**, *14*, 1429–1434.
[44] Zhang, L.; Guo, Z. Q.; Sarma, J.; Zhao, W. W.; Dai, X. M. Gradient quasi-liquid surface enabled self-propulsion of highly wetting liquids. *Adv. Funct. Mater.* **2021**, *31*, 2008614.
[45] Wang, T. Q.; Chen, H. X.; Liu, K.; Li, Y.; Xue, P. H.; Yu, Y.; Wang, S. L.; Zhang, J. H.; Kumacheva, E.; Yang, B. Anisotropic Janus Si nanopillar arrays as a microfluidic one-way valve for gas–liquid separation. *Nanoscale* **2014**, *6*, 3846–3853.
[46] Shang, L. R.; Cheng, Y.; Zhao, Y. J. Emerging droplet microfluidics. *Chem. Rev.* **2017**, *117*, 7964–8040.
[47] Kong, T.; Brien, R.; Njus, Z.; Kalwa, U.; Pandey, S. Motorized actuation system to perform droplet operations on printed plastic sheets. *Lab Chip* **2016**, *16*, 1861–1872.
[48] Li, J. Q.; Zhou, X. F.; Li, J.; Che, L. F.; Yao, J.; McHale, G.; Chaudhury, M. K.; Wang, Z. K. Topological liquid diode. *Sci. Adv.* **2017**, *3*, eaao3530.
[49] Su, B.; Wang, S. T.; Song, Y. L.; Jiang, L. A miniature droplet reactor built on nanoparticle-derived superhydrophobic pedestals. *Nano Res.* **2011**, *4*, 266–273.
[50] Higuera, F. J.; Medina, A.; Liñán, A. Capillary rise of a liquid between two vertical plates making a small angle. *Phys. Fluids* **2008**, *20*, 102102.
[51] Ponomarenko, A.; Quéré, D.; Clanet, C. A universal law for capillary rise in corners. *J. Fluid Mech.* **2011**, *666*, 146–154.
[52] Concus, P.; Finn, R. On the behavior of a capillary surface in a wedge. *Proc. Natl. Acad. Sci. USA* **1969**, *63*, 292–299.
[53] Thammanna Gurumurthy, V.; Roisman, I. V.; Tropea, C.; Garoff, S. Spontaneous rise in open rectangular channels under gravity. *J. Colloid Interface Sci.* **2018**, *527*, 151–158.
[54] Deng, D. X.; Tang, Y.; Zeng, J.; Yang, S.; Shao, H. R. Characterization of capillary rise dynamics in parallel micro V-grooves. *Int. J. Heat Mass Transf.* **2014**, *77*, 311–320.
[55] Prakash, M.; Quéré, D.; Bush, J. W. M. Surface tension transport of prey by feeding shorebirds: The capillary ratchet. *Science* **2008**, *320*, 931–934.
[56] Renvoisé, P.; Bush, J. W. M.; Prakash, M.; Quéré, D. Drop propulsion in tapered tubes. *Europhys. Lett.* **2009**, *86*, 64003.
[57] Lorenceau, L.; Quéré, D. Drops on a conical wire. *J. Fluid Mech.* **2004**, *510*, 29–45.
[58] Bico, J.; Quéré, D. Self-propelling slugs. *J. Fluid Mech.* **2002**, *467*, 101–127.
[59] Wang, Z. L.; Lin, K.; Zhao, Y. P. The effect of sharp solid edges on the droplet wettability. *J. Colloid Interface Sci.* **2019**, *552*, 563–571.
[60] Grishaev, V.; Amirfazli, A.; Chikov, S.; Lyulin, Y.; Kabov, O. Study of edge effect to stop liquid spillage for microgravity application. *Microgravity Sci. Technol.* **2013**, *25*, 27–33.
[61] Oliver, J. F.; Huh, C.; Mason, S. G. Resistance to spreading of liquids by sharp edges. *J. Colloid Interface Sci.* **1977**, *59*, 568–581.
[62] Li, J.; Guo, Z. G. Spontaneous directional transportations of water droplets on surfaces driven by gradient structures. *Nanoscale* **2018**, *10*, 13814–13831.
[63] Wu, Z. Y.; Huang, Y. Y.; Chen, X. Q.; Zhang, X. Capillary-driven flows along curved interior corners. *Int. J. Multiphase Flow* **2018**, *109*, 14–25.
[64] Berthier, J.; Brakke, K. A.; Berthier, E. A general condition for spontaneous capillary flow in uniform cross-section microchannels. *Microfluid. Nanofluid.* **2014**, *16*, 779–785.
[65] Bohn, H. F.; Federle, W. Insect aquaplaning: *Nepenthes* pitcher plants capture prey with the peristome, a fully wettable water-lubricated anisotropic surface. *Proc. Natl. Acad. Sci. USA* **2004**, *101*, 14138–14143.
[66] Taylor, B. Concerning the ascent of water between two glass plates. *Phil. Trans. Roy. Soc. Lond.* **1712**, *27*, 538.
[67] Hauksbee, F. X. An experiment touching the ascent of water between two glass plates in an hyperbolick figure. *Phil. Trans. Roy. Soc. Lond.* **1712**, *27*, 539–540.
[68] Tuteja, A.; Choi, W.; Mabry, J. M.; McKinley, G. H.; Cohen, R. E. Robust omniphobic surfaces. *Proc. Natl. Acad. Sci. USA* **2008**, *105*, 18200–18205.
[69] Bormashenko, E.; Bormashenko, Y.; Stein, T.; Whyman, G.; Bormashenko, E. Why do pigeon feathers repel water? Hydrophobicity of pennae, Cassie–Baxter wetting hypothesis and Cassie–Wenzel capillarity-induced wetting transition. *J. Colloid Interface Sci.* **2007**, *311*, 212–216.
[70] Kennedy, R. J. Directional water-shedding properties of feathers. *Nature* **1970**, *227*, 736–737.
[71] Bico, J.; Roman, B.; Moulin, L.; Boudaoud, A. Elastocapillary coalescence in wet hair. *Nature* **2004**, *432*, 690.
[72] Duprat, C.; Protière, S.; Beebe, A. Y.; Stone, H. A. Wetting of flexible fibre arrays. *Nature* **2012**, *482*, 510–513.
[73] Wang, Q. B.; Su, B.; Liu, H.; Jiang, L. Chinese brushes: Controllable liquid transfer in ratchet conical hairs. *Adv. Mater.* **2014**, *26*, 4889–4894.
[74] Yu, C. L.; Li, C. X.; Gao, C.; Dong, Z. C.; Wu, L.; Jiang, L. Time-dependent liquid transport on a biomimetic topological surface. *ACS Nano* **2018**, *12*, 5149–5157.
[75] Wang, J.; Yi, S. Z.; Yang, Z. L.; Chen, Y.; Jiang, L. L.; Wong, C. P. Laser direct structuring of bioinspired spine with backward microbarbs and hierarchical microchannels for ultrafast water transport and efficient fog harvesting. *ACS Appl. Mater. Interfaces* **2020**, *12*, 21080–21087.
[76] Lv, J. A.; Liu, Y. Y.; Wei, J.; Chen, E. Q.; Qin, L.; Yu, Y. L. Photocontrol of fluid slugs in liquid crystal polymer microactuators. *Nature* **2016**, *537*, 179–184.
[77] Xu, B.; Zhu, C. Y.; Qin, L.; Wei, J.; Yu, Y. L. Light-directed liquid manipulation in flexible bilayer microtubes. *Small* **2019**, *15*, 1901847.
[78] Feng, W. Q.; Ueda, E.; Levkin, P. A. Droplet microarrays: From surface patterning to high-throughput applications. *Adv. Mater.* **2018**, *30*, 1706111.
[79] Ichimura, K.; Oh, S. K.; Nakagawa, M. Light-driven motion of liquids on a photoresponsive surface. *Science* **2000**, *288*, 1624–1626.
[80] An, S.; Zhu, M. Y.; Gu, K.; Jiang, M. D.; Shen, Q. C.; Fu, B. W.; Song, C. Y.; Tao, P.; Deng, T.; Shang, W. Light-driven motion of water droplets with directional control on nanostructured surfaces. *Nanoscale* **2020**, *12*, 4295–4301.
[81] Xiao, Y.; Zarghami, S.; Wagner, K.; Wagner, P.; Gordon, K. C.; Florea, L.; Diamond, D.; Officer, D. L. Moving droplets in 3D using light. *Adv. Mater.* **2018**, *30*, 1801821.
[82] Kwon, G.; Panchanathan, D.; Mahmoudi, S. R.; Gondal, M. A.; McKinley, G. H.; Varanasi, K. K. Visible light guided manipulation of liquid wettability on photoresponsive surfaces. *Nat. Commun.* **2017**, *8*, 14968.
[83] Wang, S. L.; Zhou, R. M.; Hou, Y. Q.; Wang, M.; Hou, X. Photochemical effect driven fluid behavior control in microscale pores and channels. *Chin. Chem. Lett.* **2022**, *33*, 3650–3656.
[84] Cao, M. Y.; Jin, X.; Peng, Y.; Yu, C. M.; Li, K.; Liu, K. S.; Jiang, L. Unidirectional wetting properties on multi-bioinspired magnetocontrollable slippery microcilia. *Adv. Mater.* **2017**, *29*, 1606869.
[85] Lei, W. W.; Hou, G. L.; Liu, M. J.; Rong, Q. F.; Xu, Y. C.; Tian, Y.; Jiang, L. High-speed transport of liquid droplets in magnetic tubular microactuators. *Sci. Adv.* **2018**, *4*, eaau8767.
[86] Liu, H.; Zheng, S.; Yang, X.; Liao, W. B.; Wang, C.; Miao, W. N.; Tang, J. Y.; Wang, D. Y.; Tian, Y. Magnetic actuation multifunctional platform combining microdroplets delivery and stirring. *ACS Appl. Mater. Interfaces* **2019**, *11*, 47642–47648.
[87] García-Torres, J.; Calero, C.; Sagués, F.; Pagonabarraga, I.; Tierno, P. Magnetically tunable bidirectional locomotion of a self-assembled nanorod–sphere propeller. *Nat. Commun.* **2018**, *9*, 1663.
[88] Wang, W. D.; Timonen, J. V. I.; Carlson, A.; Drotlef, D. M.; Zhang, C. T.; Kolle, S.; Grinthal, A.; Wong, T. S.; Hatton, B.; Kang, S. H. et al. Multifunctional ferrofluid-infused surfaces with reconfigurable multiscale topography. *Nature* **2018**, *559*, 77–82.
[89] Guo, J. C.; Wang, D. H.; Sun, Q. Q.; Li, L. X.; Zhao, H. X.; Wang, D. D.; Cui, J. X.; Chen, L. Q.; Deng, X. Omni-liquid droplet manipulation platform. *Adv. Mater. Interfaces* **2019**, *6*, 1900653.

[90] Liu, J.; Xu, X.; Lei, Y.; Zhang, M. C.; Sheng, Z. Z.; Wang, H. M.; Cao, M.; Zhang, J.; Hou, X. Liquid gating meniscus-shaped deformable magnetoelastic membranes with self-driven regulation of gas/liquid release. *Adv. Mater.* **2022**, *34*, 2107327.
[91] Li, J. Q.; Zhou, X. F.; Tao, R.; Zheng, H. X.; Wang, Z. K. Directional liquid transport from the cold region to the hot region on a topological surface. *Langmuir* **2021**, *37*, 5059–5065.
[92] Li, C. X.; Yu, C. L.; Hao, D. Z.; Wu, L.; Dong, Z. C.; Jiang, L. Smart liquid transport on dual biomimetic surface via temperature fluctuation control. *Adv. Funct. Mater.* **2018**, *28*, 1707490.
[93] Li, J.; Hou, Y. M.; Liu, Y. H.; Hao, C. L.; Li, M. F.; Chaudhury, M. K.; Yao, S. H.; Wang, Z. K. Directional transport of high-temperature Janus droplets mediated by structural topography. *Nat. Phys.* **2016**, *12*, 606–612.
[94] Yakhshi-Tafti, E.; Cho, H. J.; Kumar, R. Droplet actuation on a liquid layer due to thermocapillary motion: Shape effect. *Appl. Phys. Lett.* **2010**, *96*, 264101.
[95] Yarin, A. L.; Liu, W. X.; Reneker, D. H. Motion of droplets along thin fibers with temperature gradient. *J. Appl. Phys.* **2002**, *91*, 4751–4760.
[96] Al-Sharafi, A.; Yilbas, B. S.; Ali, H. Water droplet mobility on a hydrophobic surface under a thermal radiative heating. *Appl. Therm. Eng.* **2018**, *128*, 92–106.
[97] Han, Y. H.; Zhang, Y. M.; Zhang, M. C.; Chen, B. Y.; Chen, X. Y.; Hou, X. Photothermally induced liquid gate with navigation control of the fluid transport. *Fundam. Res.* **2021**, *1*, 800–806.
[98] Sun, Q. Q.; Wang, D. H.; Li, Y. N.; Zhang, J. H.; Ye, S. J.; Cui, J. X.; Chen, L. Q.; Wang, Z. K.; Butt, H. J.; Vollmer, D. et al. Surface charge printing for programmed droplet transport. *Nat. Mater.* **2019**, *18*, 936–941.
[99] Li, N.; Yu, C. L.; Dong, Z. C.; Jiang, L. Finger directed surface charges for local droplet motion. *Soft Matter* **2020**, *16*, 9176–9182.
[100] Yang, X. L.; Li, Y. M.; Zheng, H. X.; Lu, Y. Saturated surface charging on micro/nanoporous polytetrafluoroethylene for droplet manipulation. *ACS Appl. Nano Mater.* **2022**, *5*, 3342–3351.
[101] Wang, F. X.; Sun, Y. Y.; Zong, G. G.; Liang, W. Y.; Yang, B.; Guo, F. Z.; Yangou, C.; Wang, Y. B.; Zhang, Z. C. Electrothermally assisted surface charge density gradient printing to drive droplet transport. *ACS Appl. Mater. Interfaces* **2022**, *14*, 3526–3535.
[102] Wang, Q. B.; Xu, B. J.; Hao, Q.; Wang, D.; Liu, H.; Jiang, L. *In situ* reversible underwater superwetting transition by electrochemical atomic alternation. *Nat. Commun.* **2019**, *10*, 1212.
[103] Wang, J.; Sun, L. Y.; Zou, M. H.; Gao, W.; Liu, C. H.; Shang, L. R.; Gu, Z. Z.; Zhao, Y. J. Bioinspired shape-memory graphene film with tunable wettability. *Sci. Adv.* **2017**, *3*, e1700004.
[104] Gao, W.; Wang, J.; Zhang, X. X.; Sun, L. Y.; Chen, Y. P.; Zhao, Y. J. Electric-tunable wettability on a paraffin-infused slippery pattern surface. *Chem. Eng. J.* **2020**, *381*, 122612.
[105] Lu, X. Y.; Kong, Z.; Xiao, G. Z.; Teng, C.; Li, Y. N.; Ren, G. Y.; Wang, S. B.; Zhu, Y.; Jiang, L. Polypyrrole whelk-like arrays toward robust controlling manipulation of organic droplets underwater. *Small* **2017**, *13*, 1701938.
[106] Mannetje, D.; Ghosh, S.; Lagraauw, R.; Otten, S.; Pit, A.; Berendsen, C.; Zeegers, J.; van den Ende, D.; Mugele, F. Trapping of drops by wetting defects. *Nat. Commun.* **2014**, *5*, 3559.
[107] Pan, Z.; Pitt, W. G.; Zhang, Y. M.; Wu, N.; Tao, Y.; Truscott, T. T. The upside–down water collection system of *Syntrichia caninervis*. *Nat. Plants* **2016**, *2*, 16076.
[108] Li, C. X.; Yu, C. L.; Zhou, S.; Dong, Z. C.; Jiang, L. Liquid harvesting and transport on multiscaled curvatures. *Proc. Natl. Acad. Sci. USA* **2020**, *117*, 23436–23442.
[109] Li, C. X.; Dai, H. Y.; Gao, C.; Wang, T.; Dong, Z. C.; Jiang, L. Bioinspired inner microstructured tube controlled capillary rise. *Proc. Natl. Acad. Sci. USA* **2019**, *116*, 12704–12709.
[110] Teh, S. Y.; Lin, R.; Hung, L. H.; Lee, A. P. Droplet microfluidics. *Lab Chip* **2008**, *8*, 198–220.
[111] Guo, M. T.; Rotem, A.; Heyman, J. A.; Weitz, D. A. Droplet microfluidics for high-throughput biological assays. *Lab Chip* **2012**, *12*, 2146–2155.
[112] Jiao, Z. J.; Nguyen, N. T.; Huang, X. Y.; Ang, Y. Z. Reciprocating thermocapillary plug motion in an externally heated capillary. *Microfluid. Nanofluid.* **2006**, *3*, 39–46.
[113] Li, C. X.; Wu, L.; Yu, C. L.; Dong, Z. C.; Jiang, L. Peristome-mimetic curved surface for spontaneous and directional separation of micro water-in-oil drops. *Angew. Chem., Int. Ed.* **2017**, *56*, 13623–13628.
[114] Narayanamurthy, V.; Nagarajan, S.; Firus Khan, A. Y.; Samsuri, F.; Sridhar, T. M. Microfluidic hydrodynamic trapping for single cell analysis: Mechanisms, methods and applications. *Anal. Methods* **2017**, *9*, 3751–3772.
[115] Nilsson, J.; Evander, M.; Hammarström, B.; Laurell, T. Review of cell and particle trapping in microfluidic systems. *Anal. Chim. Acta* **2009**, *649*, 141–157.
[116] Lin, C. M.; Lai, Y. S.; Liu, H. P.; Chen, C. Y.; Wo, A. M. Trapping of bioparticles via microvortices in a microfluidic device for bioassay applications. *Anal. Chem.* **2008**, *80*, 8937–8945.
[117] Olanrewaju, A.; Beaugrand, M.; Yafia, M.; Juncker, D. Capillary microfluidics in microchannels: From microfluidic networks to capillaric circuits. *Lab Chip* **2018**, *18*, 2323–2347.
[118] Zhou, S.; Yu, C. L.; Li, C. X.; Jiang, L.; Dong, Z. C. Droplets crawling on peristome-mimetic surfaces. *Adv. Funct. Mater.* **2020**, *30*, 1908066.
[119] Li, C. X.; Li, N.; Zhang, X. S.; Dong, Z. C.; Chen, H. W.; Jiang, L. Uni-directional transportation on peristome-mimetic surfaces for completely wetting liquids. *Angew. Chem., Int. Ed.* **2016**, *55*, 14988–14992.
[120] Tang, X. X.; Liu, H. W.; Xiao, L.; Zhou, M. L.; Bai, H. Y.; Fang, J. H.; Cui, Z. H.; Cheng, H.; Li, G. Q.; Zhang, Y. B. et al. A hierarchical origami moisture collector with laser-textured microchannel array for a plug-and-play irrigation system. *J. Mater. Chem. A* **2021**, *9*, 5630–5638.
[121] Li, J.; Zhou, Y. L.; Cong, J. P.; Xu, C. Y.; Ren, L. Q. Bioinspired integrative surface with hierarchical texture and wettable gradient-driven water collection. *Langmuir* **2020**, *36*, 14737–14747.